



Crystal structure of the GDP-bound GTPase domain of Rab5a from *Leishmania donovani*

Muhammad Zohib, Diva Maheshwari, Ravi Kant Pal, Stefanie Freitag-Pohl, Bichitra Kumar Biswal, Ehmke Pohl and Ashish Arora

Acta Cryst. (2020). F76, 544–556



IUCr Journals
CRYSTALLOGRAPHY JOURNALS ONLINE

Copyright © International Union of Crystallography

Author(s) of this article may load this reprint on their own web site or institutional repository provided that this cover page is retained. Republication of this article or its storage in electronic databases other than as specified above is not permitted without prior permission in writing from the IUCr.

For further information see <https://journals.iucr.org/services/authorrights.html>



Crystal structure of the GDP-bound GTPase domain of Rab5a from *Leishmania donovani*

Muhammad Zohib,^{a,b} Diva Maheshwari,^a Ravi Kant Pal,^c Stefanie Freitag-Pohl,^d Bichitra Kumar Biswal,^c Ehmke Pohl^d and Ashish Arora^{a,b*}

^aMolecular and Structural Biology Division, CSIR – Central Drug Research Institute, Lucknow 226 031, India, ^bAcademy of Scientific and Innovative Research (AcSIR), Ghaziabad 201 002, India, ^cX-ray Crystallography Facility, National Institute of Immunology, New Delhi 110 067, India, and ^dDepartment of Chemistry, Durham University, Durham DH1 3LE, United Kingdom. *Correspondence e-mail: ashish_arora@cdri.res.in

Received 11 July 2020

Accepted 13 October 2020

Edited by M. Rudolph, F. Hoffmann-La Roche Ltd, Switzerland

Keywords: *Leishmania donovani*; fluid-phase endocytosis; early endosomes; Rab5a; crystal structure.

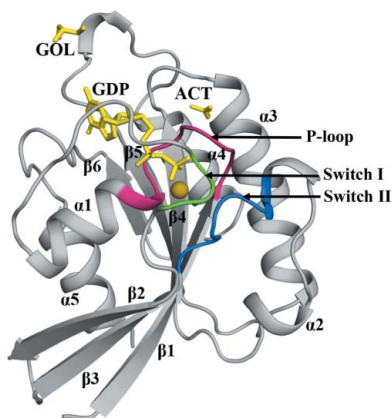
PDB reference: GDP-bound GTPase domain of Rab5a, 6l6o

Supporting information: this article has supporting information at journals.iucr.org/f

Eukaryotic Rab5s are highly conserved small GTPase-family proteins that are involved in the regulation of early endocytosis. *Leishmania donovani* Rab5a regulates the sorting of early endosomes that are involved in the uptake of essential nutrients through fluid-phase endocytosis. Here, the 1.80 Å resolution crystal structure of the N-terminal GTPase domain of *L. donovani* Rab5a in complex with GDP is presented. The crystal structure determination was enabled by the design of specific single-site mutations and two deletions that were made to stabilize the protein for previous NMR studies. The structure of LdRab5a shows the canonical GTPase fold, with a six-stranded central mixed β -sheet surrounded by five α -helices. The positions of the Switch I and Switch II loops confirm an open conformation, as expected in the absence of the γ -phosphate. However, in comparison to other GTP-bound and GDP-bound homologous proteins, the Switch I region traces a unique disposition in LdRab5a. One magnesium ion is bound to the protein at the GTP-binding site. Molecular-dynamics simulations indicate that the GDP-bound structure exhibits higher stability than the apo structure. The GDP-bound LdRab5a structure presented here will aid in efforts to unravel its interactions with its regulators, including the guanine nucleotide-exchange factor, and will lay the foundation for a structure-based search for specific inhibitors

1. Introduction

Leishmania donovani, a causative agent of the disease visceral leishmaniasis, lives a digenetic life between phlebotomine sand flies and human beings. While the parasites adopt a procyclic promastigote form in the insects, in human hosts they reside in the highly acidic environment of macrophages within the parasitophorous vacuole as the ovoid amastigote form (Real & Mortara, 2012; Young & Kima, 2019). In both of the forms, essential nutrients and other molecules are accessed through various processes including endocytosis. The transport of endocytic cargoes is carried out through a series of coordinated and specific vesicle-fusion events (Doherty & McMahon, 2009). This specific targeting and transport of internalized cargoes is highly regulated by small GTP-binding members of the Rab family (Markgraf *et al.*, 2007). *Leishmania* has a robust endocytosis system for nutrient uptake and defense from the humoral arm of the host immune system. One essential key pathway that is absent in *Leishmania* is the biosynthesis of heme, as it lacks most of the required enzymes (Kořený *et al.*, 2010; Orrego *et al.*, 2019). An essential process for the acquisition of heme involves the transport of the



© 2020 International Union of Crystallography

hemoglobin receptor to the flagellar pocket region, the rapid endocytosis of hemoglobin and its transport to the lysosomes for degradation. These steps are regulated by various Rab proteins (Sengupta *et al.*, 1999; Rastogi *et al.*, 2016).

Rab proteins are members of the largest subfamily of small GTPases. They are highly conserved and share about 30–75% homology from yeast to mammals (Zahraoui *et al.*, 1989). More than 70 Rabs have been identified in humans to date. All Rabs have conserved N- and C-terminal regions which have distinct functions. The N-terminal domain has a canonical GTPase fold, while the long C-terminal unstructured region, which terminates preferentially in a CC or CXC sequence, is the site of geranylgeranylation and consequently of anchorage to the membrane (Leung *et al.*, 2006). The GTPase fold is made up of a central six-stranded β -sheet, which is surrounded by five α -helices. Rab-family members contain five amino-acid segments that contain highly conserved functional residues. These are labeled G1–G5 and connect some of the α -helices and β -strands. Of these, the G1, G2 and G3 loops, which are commonly known as the P-loop, Switch I and Switch II, respectively, are important for binding to the phosphate moiety of the GTP and for the GTPase activity of the protein (Stenmark & Olkkonen, 2001).

Rab proteins interchange between a cytosolic inactive form and a membrane-bound active form, depending on their nucleotide-binding status (Vetter & Wittinghofer, 2001). All newly synthesized Rabs are recognized by Rab escort protein (REP) and are presented to Rab geranylgeranyltransferase (Rab GGTase), which geranylgeranylates the Rab at one or two C-terminal cysteine residues (Anant *et al.*, 1998; Goody *et al.*, 2017). REP exhibits a higher affinity for GDP-bound Rab in comparison to GTP-bound Rab, but a lower affinity for prenylated Rab in comparison to free Rab. Prenylated Rab is recruited by specific membranes through membrane-localized guanine-exchange factors (GEFs) and other factors (Lange-meyer *et al.*, 2018; Blümer *et al.*, 2013). GEF also stimulates the release of GDP from membrane-anchored prenylated Rab protein, with concomitant binding of GTP, which is present in the cytosol at a tenfold higher concentration than GDP (Ullrich *et al.*, 1994). Once in the GTP-bound form, membrane-anchored Rab proteins adopt their active conformation and begin to recruit and interact with specific effector proteins and consequently affect further downstream events. Distinct Rabs function as different components of cellular trafficking by targeting specific membranes, even though they share an overall similar fold (Guo *et al.*, 2013). Targeting to specific membranes is related to specificity towards regulatory and effector proteins. A small number of subfamily-specific nonconserved residues provide the specificity for particular partners (Delprato & Lambright, 2007; Zhu *et al.*, 2004). However, all Rab proteins go through nucleotide-exchange cycles in order to change their conformation between the active and inactive forms. Restructuring of the effector-binding site is coupled to nucleotide exchange. A GTPase-activating protein (GAP) converts Rab back to its inactive GDP-bound form. The extraction of inactive Rab from the membrane and its diffusion back to membrane compartments

for another round of activation is enabled by GDP dissociation inhibitor (GDI), an evolutionarily conserved REP paralog which has a higher affinity for GDP-bound and prenylated Rab (Gavriljuk *et al.*, 2013; Pylypenko *et al.*, 2018).

In *Leishmania*, more than 11 Rabs have been identified, including Rab1, Rab4, Rab5, Rab6, Rab7 and Rab11 (Chauhan *et al.*, 2015). Higher eukaryotes possess three isoforms of the Rab5 protein, namely Rab5a, Rab5b and Rab5c, while in *Leishmania* only two isoforms, Rab5a and Rab5b, have been identified. Rab5a and Rab5b in *Leishmania* share ~62% similarity to each other and are reported to function at an early endocytic stage. In *L. donovani*, Rab5b is involved in the regulation of hemoglobin uptake via receptor-mediated endocytosis, while Rab5a has been shown to mediate HRP uptake through fluid-phase endocytosis. Null mutants of both Rab5a and Rab5b have been reported to be lethal to the parasite (Rastogi *et al.*, 2016). Therefore, there is clearly potential for these Rab proteins to become novel drug targets. It is intriguing that a number of Rab proteins are targets for cancer and other diseases (Hutagalung & Novick, 2011; Qin *et al.*, 2017). However, so far, there is no drug targeting any protozoan Rab5 or Rab protein.

Here, we present the crystal structure of the GTPase domain of Rab5a from *L. donovani* (LdRab5a) in the presence of GDP. The structure has been compared with GDP-bound and GTP-bound structures of homologous Rab5 proteins, which shows that the Switch I region adopts a unique disposition in LdRab5a. Molecular-dynamics (MD) simulations show that GDP imparts conformational stability to the apo LdRab5a structure. The LdRab5a structure presented here will be helpful in understanding the basis of interaction with effectors which only bind to the GDP-bound form of Rab.

2. Materials and methods

2.1. Purification of LdRab5a

The cloning and expression of stabilized LdRab5a has been described previously (Maheshwari *et al.*, 2018). For stabilization, Q93L, P58D, P59G and C107S mutations and $\Delta 60$ –79 and $\Delta 196$ –235 deletions were incorporated sequentially, with monitoring of the linewidths and dispersion in the ^{15}N - ^1H -HSQC spectrum of the protein over a period of nine or more days. The residues of the stabilized LdRab5a mutant are numbered consecutively from 1 to 175. However, in the crystal structure only the residues from Ala11 to Leu175 are visible. LdRab5a was recombinantly expressed in *Escherichia coli* as a GST-fusion protein with a thrombin protease cleavage site between the two proteins, as described previously (Maheshwari *et al.*, 2018). Purification of the protein was performed as follows. Briefly, *E. coli* cells expressing GST-LdRab5a were lysed and the supernatant from the lysed cells was incubated overnight at 4°C with Glutathione Agarose 4B Beads (Machary Nagel) that had been pre-equilibrated with buffer A (50 mM Tris-HCl pH 8.0, 100 mM NaCl, 5 mM MgCl₂, 1 mM GTP). After binding, the beads were packed into a small column and washed sequentially with buffer A and buffer B

(50 mM Tris–HCl pH 7.5, 100 mM NaCl, 5 mM MgCl₂, 1 mM GTP). On-column digestion was performed to cleave the GST tag using thrombin protease (1 unit per milligram of protein; Calbiochem, San Diego, California, USA) at 22°C for 12 h. The cleaved LdRab5a protein was collected in the flow-through. The protein was dialyzed against 20 mM Tris–HCl buffer pH 8.3 containing 50 mM NaCl, 5 mM MgCl₂, 1 mM DTT and 1 mM GTP and was concentrated to 8 mg ml^{−1} using 3 kDa molecular-weight cutoff centrifugal concentrator units (Millipore India). The concentrated protein was further purified by size-exclusion chromatography on a Superdex 75 10/300 GL column (GE Healthcare, Chicago, Illinois, USA) using a fast-performance liquid-chromatography system (Bio-Rad BioLogic Duo Flow; Bio-Rad, Hercules, California, USA). The purity of the protein when checked by 15% SDS–PAGE was greater than 95%.

2.2. Crystallization

The purified LdRab5a protein was extensively dialyzed against buffer C (20 mM Tris–HCl pH 8.3, 50 mM NaCl, 5 mM MgCl₂, 1 mM DTT, 1 mM GTP) and was concentrated to 10 mg ml^{−1} using 3 kDa molecular-weight cutoff concentrator units (Millipore India). Protein crystallization was optimized with the Hampton Research Crystal Screen and Crystal Screen 2 kits using the hanging-drop vapor-diffusion method (Jancarik & Kim, 1991) in 24-well plates (Corning, USA). Crystallization drops were set up by mixing equal volumes of protein solution and mother liquor (2 µl each) and were equilibrated against 500 µl reservoir solution. The crystallization plates were incubated at 277 and 295 K. After obtaining initial hits, protein crystals with high diffraction quality were grown using a reservoir solution consisting of 0.1 M Tris–HCl pH 8.5, 0.2 M ammonium acetate, 15% polyethylene glycol 3350 at 277 K in about 20 days. Prior to setting up crystallization, the protein was incubated with an additional 1 mM GTP (in buffer C) for 20 min.

2.3. X-ray diffraction and structure determination

For X-ray data collection, crystals of LdRab5a were soaked in a cryoprotectant consisting of 20% glycerol in the reservoir solution and were picked from the drops using CryoLoops (Hampton Research). The crystals were flash-cooled in a nitrogen stream at 100 K. X-ray diffraction data were collected to a resolution of 1.8 Å using a Rigaku FR-E+ SuperBright X-ray data-collection system with an R-AXIS IV++ detector at the X-ray Diffraction Facility, National Institute of Immunology, New Delhi, India. The crystal-to-detector distance was kept at 125 mm during the collection of diffraction data for each frame. A total of 403 frames were collected and the oscillation steps were kept at 0.75°, with an exposure time of 120 s per frame. The reflections were indexed, integrated and scaled in *HKL*-2000. The crystal was indexed in the trigonal space group *P*₃21, with unit-cell parameters *a* = *b* = 58.02, *c* = 103.42 Å, α = β = 90, γ = 120°. Data-collection statistics are summarized in Table 1. The LdRab5a protein structure was determined by the molecular-

Table 1
X-ray data-collection and refinement statistics.

Values in parentheses are for the outer shell.

Data collection	
Wavelength (Å)	1.5418
Resolution range (Å)	35.0–1.80 (1.86–1.80)
Space group	<i>P</i> ₃ 21
<i>a</i> , <i>b</i> , <i>c</i> (Å)	58.02, 58.02, 103.42
α , β , γ (°)	90, 90, 120
No. of molecules in the asymmetric unit	1
Total reflections	287720
Unique reflections	19056
Multiplicity	15.1 (8.8)
Completeness (%)	98.9 (89.7)
Mean <i>I</i> / σ (<i>I</i>)	55.08 (2.09)
Wilson <i>B</i> factor (Å ²)	29.6
<i>R</i> _{merge} [†] (%)	5.7 (74.8)
<i>R</i> _{meas} (%)	5.9 (78.4)
CC _{1/2} (%)	100 (90.9)
Refinement	
Resolution	24.4–1.80 (1.85–1.80)
<i>R</i> _{work} [‡] (%)	16.5
<i>R</i> _{free} [‡] (%)	20.3
No. of non-H atoms	
Total	1447
Protein	1284
Ligands	39
Mg	1
Water	124
R.m.s. deviations	
Bond lengths (Å)	0.019
Angles (Å)	2.27
Ramachandran plot	
Most favored (%)	97.55
Allowed (%)	2.45
Outliers (%)	0
<i>MolProbity</i> clashscore	5.65
Average <i>B</i> factors (Å ²)	
Overall	37.95
Macromolecule	37.44
Ligands	37.66
Solvent	43.39
PDB code	6l6o

$$\dagger R_{\text{merge}} = \frac{\sum_{hkl} \sum_i |I_i(hkl) - \langle I(hkl) \rangle|}{\sum_{hkl} \sum_i I_i(hkl)} \quad \ddagger R_{\text{work}} = \frac{\sum_{hkl} ||F_{\text{obs}}| - |F_{\text{calc}}||}{\sum_{hkl} |F_{\text{obs}}|}$$

replacement method with *Phaser* (McCoy *et al.*, 2007) using the structure of human Rab5b (HsRab5b; PDB entry 2hei; Structural Genomics Consortium, unpublished work) as the search model. The amino-acid sequence of LdRab5a shares 52% identity with that of HsRab5b. The structure was solved with one molecule in the asymmetric unit, a Matthews coefficient of 2.56 Å³ Da^{−1} (Matthews, 1968) and a solvent content of 52.05%.

The initial model obtained from *Phaser* was first refined as a rigid body, followed by restrained and individual isotropic temperature refinement using *REFMAC5* (Murshudov *et al.*, 2011). Model building was carried out using *Coot* (Emsley & Cowtan, 2004; Emsley *et al.*, 2010). The refined model was further subjected to simulated-annealing refinement using *Phenix* (Liebschner *et al.*, 2019), and a composite OMIT map (2|*F*_o| − |*F*_c|) was calculated and checked at the end of the refinement. Iterative rounds of structure refinement and model building were carried out in *REFMAC5* and *Coot*, respectively, until the model was completely built. In the final rounds of refinement, TLS and anisotropic *B*-factor restraints

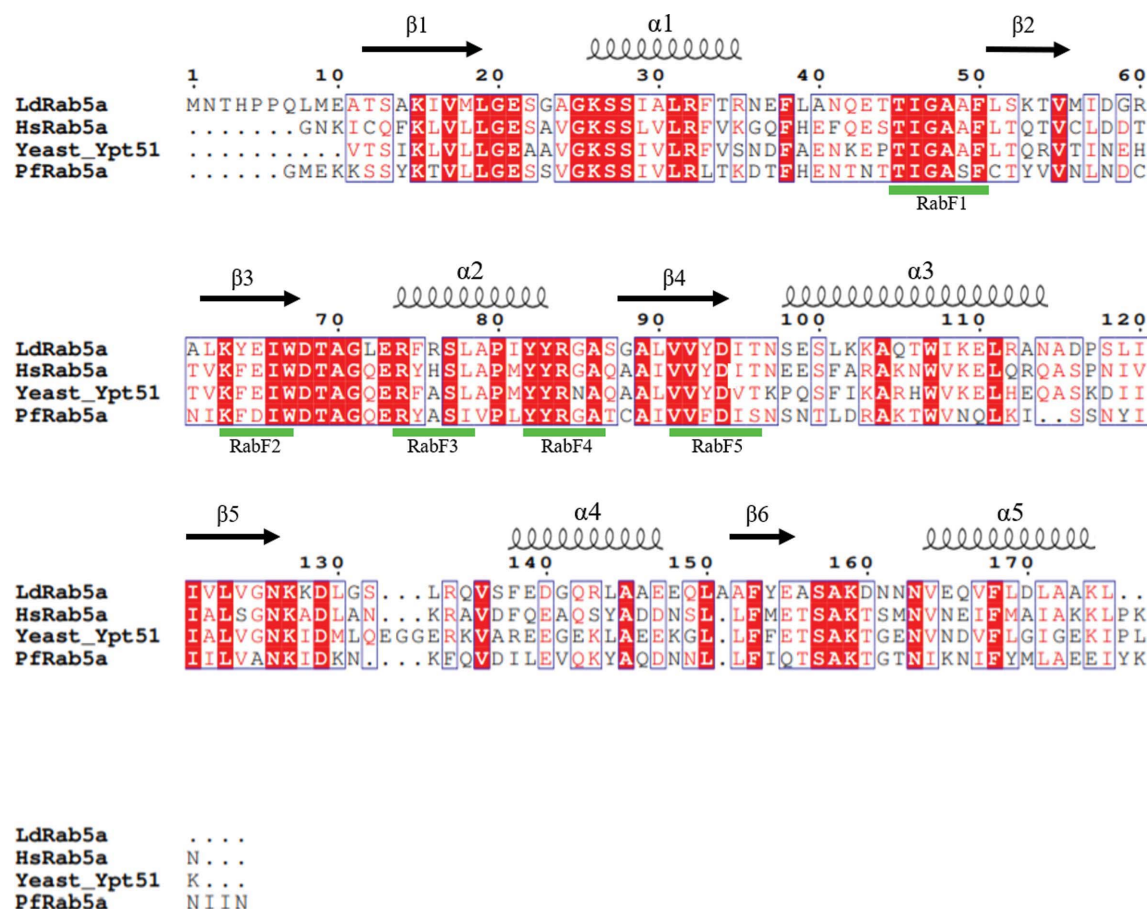


Figure 1
 Multiple sequence alignment of LdRab5a with other Rab sequences. Consecutively numbered sequences were derived from the crystal structures of LdRab5a (PDB entry 6l6o), human Rab5a (PDB entry 1n6h), yeast Ypt51 (PDB entry 1ek0) and *Plasmodium falciparum* Rab5a (PDB entry 3clv). Conserved regions are shown in red and Rab family-specific motifs are highlighted by green ribbons.

were applied for the entire chain. Poor electron density was observed for the side chains of three residues, Asn41, Ile57 and Lys174, but the atoms of these side chains were added in order to better trace the main chain. The final model of LdRab5a consists of 165 residues, one magnesium ion, one glycerol molecule, one acetate molecule and 124 solvent molecules, with an *R* factor of 16.5% and an *R*_{free} of 20.3% (Brünger, 1993). Ramachandran plot analysis of the final model using *PROCHECK* (Laskowski *et al.*, 1993) shows that 92.7% of the residues lie in the most favored region, while 7.3% of the residues lie in the allowed region. Structure-related figures were generated using *PyMOL* (Schrödinger). The final refined atomic coordinates have been deposited in the Protein Data Bank (PDB) as PDB entry 6l6o. Details of the crystal structure determination are summarized in Table 1.

2.4. MD simulations

MD simulations were performed using *GROMACS* (version 5.1.2). The GROMOS96 54a7 force field was applied to parameterize the protein both in the absence and the presence of GDP (Schmid *et al.*, 2011). For simulation in the presence of GDP, topology and other parameters for GDP

were generated using the *PRODRG* online server (<http://prodr1.dyndns.org/>). For solvation of the system, a cubic SPC water box was employed followed by charge neutralization. Prior to adding the positional restraints for GDP, energy minimization was performed using the steepest-descent algorithm. System equilibration was carried out at 300 K for 100 ps using the NVT ensemble and for 100 ps using the NPT ensemble. Production molecular-dynamics simulations were performed for 100 ns for both the GDP-bound and the apo structure. After simulation, the root-mean-square deviation (r.m.s.d.) and root-mean-square fluctuation (r.m.s.f.) per residue were calculated and compared.

3. Results

3.1. Multiple sequence alignment of LdRab5a with other Rab5 proteins

LdRab5a was stabilized through Q93L, P58D, P59G and C107S mutations and Δ60–79 and Δ196–235 deletions. After these modifications, the residues of the stabilized LdRab5a mutant were numbered consecutively from 1 to 175. Multiple sequence alignment of the stabilized LdRab5a sequence with

sequences from the crystal structures of HsRab5a (PDB entry 1n6h; Zhu *et al.*, 2003), yeast Ypt51 (PDB entry 1ek0; Esters *et al.*, 2000) and PfRab5a (PDB entry 3clv; Structural Genomics Consortium, unpublished work) was performed using *ClustalW* (<http://www.ebi.ac.uk/clustalomega/>) and is shown in Fig. 1. The conserved residues, which include the nucleotide-binding P-loop (RabF1) and switch regions (RabF2 and RabF3), along with Rab5 family-specific sequences (RabF4 and RabF5), are highlighted under the sequence with green ribbons. PfRab5a has an extra stretch of 37 residues (Ile67–Leu103) similar to LdRab5a (the deleted 20-residue stretch Pro60–Met79) at the same position between $\beta 2$ and $\beta 3$. HsRab5a and yeast Ypt51 do not possess this loop.

3.2. Crystal structure of the GDP-bound GTPase domain of LdRab5a

The structure of LdRab5a (PDB entry 6l6o) was solved at 1.80 Å resolution (Table 1). Although the protein was crystallized in the presence of GTP, we found one molecule of GDP and one magnesium ion bound to the protein. Additionally, one glycerol molecule and one acetate molecule were also found in the LdRab5a crystal structure. In the crystal structure, no electron density was found for the initial ten residues (Met1–Glu10) at the N-terminus, which were omitted from the structure.

The crystal structure of LdRab5a, as shown in Fig. 2, displays the canonical Rab topology in which a six-stranded central mixed β -sheet is surrounded by five α -helices. The

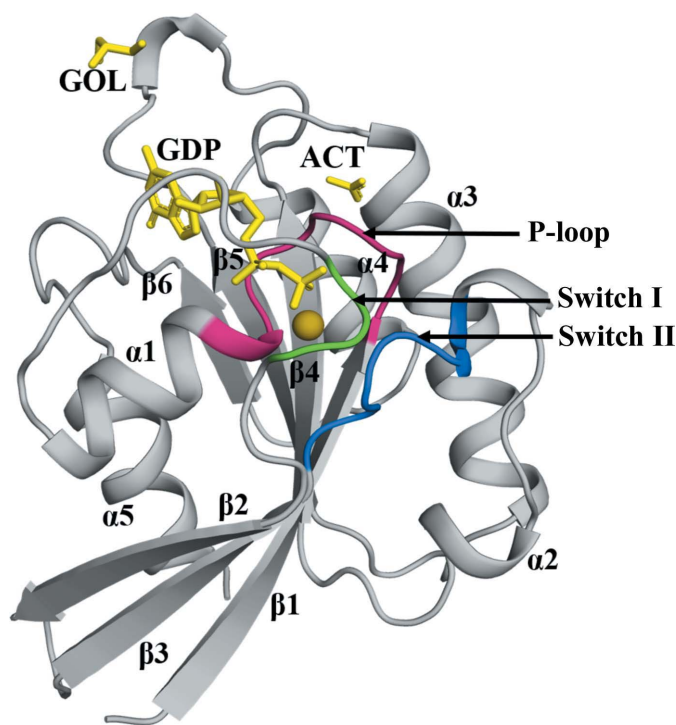


Figure 2
Crystal structure of LdRab5a in the presence of GDP. Color scheme: LdRab5a, gray; phosphate-binding loop, warm pink; Switch I, green; Switch II, marine; GTP, acetate, glycerol, yellow; Mg, olive.

various secondary-structure elements in topological order are as follows: $\beta 1$ (12–21), $\alpha 1$ (25–36), $\beta 2$ (49–57), $\beta 3$ (60–68), $\alpha 2$ (71–84), $\beta 4$ (87–95), $\alpha 3$ (97–115), $\beta 5$ (120–126), $\alpha 4$ (137–148), $\beta 6$ (152–156), $\alpha 5$ (163–175). With the exception of strands $\beta 2$ and $\beta 3$, all β -strands run parallel to each other. Some of the β -strands and α -helices are connected by functionally important loops, which are highly conserved in Rab-GTPases and are conventionally labeled G1–G5, as per the Ras-superfamily nomenclature. The G1 loop, which is also called the P-loop, interacts with the α - and β -phosphates of GDP and has the consensus sequence 20 GESGAGKS 27 . The G2 or Switch I loop and the G3 or Switch II loop contain the conserved sequences 44 TTI 46 and 68 DTAGLE 73 , respectively. Together, these loops adopt an open conformation because of the absence of the γ -phosphate. Along with the phosphate-binding loop (P-loop), these two loops share important interactions with the nucleotide γ -phosphate for the GTPase activity of the protein.

Furthermore, Switch I, Switch II and the inter-switch regions are primarily involved in the interaction with effector proteins, as observed in the crystal structures of various Rab proteins bound to their effectors (Zhu *et al.*, 2004; Eathiraj *et al.*, 2005; Mishra *et al.*, 2010). The crystal structure contains GDP in the pocket formed by the G1–G3 loops, which is stabilized by hydrogen bonds to various residues contributed by these loops and water molecules.

Additionally, one Mg^{2+} ion was also found in the crystal structure. This Mg^{2+} (Mg1A) is located in the GTP-binding pocket and is hexacoordinated by Ser27, the β -phosphoryl group of GDP and water molecules, as shown in Fig. 3. However, the segment conventionally designated helix $\alpha 2$ was partially unfolded and was divided into two α -helical regions, 71–76 and 79–86, which were connected by an elongated stretch. Such a break in helix $\alpha 2$ is also observed in all other GDP-bound Rab GTPases. This helix undergoes a partial deformation, which is coupled to nucleotide exchange, and

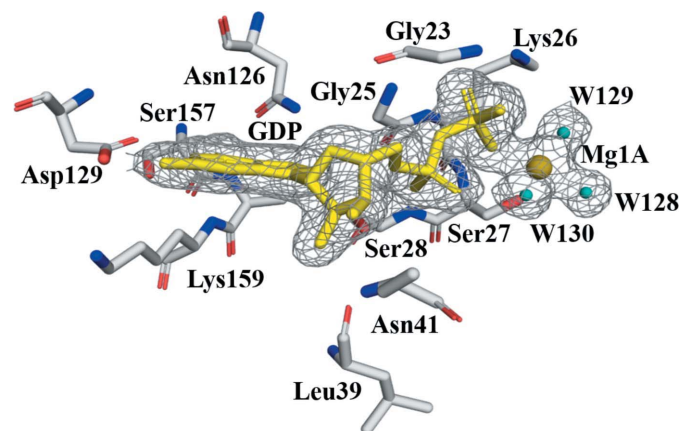


Figure 3
Interaction stabilizing GDP and magnesium in the LdRab5a crystal structure. GDP (yellow) in LdRab5a with neighboring residues (C atoms in gray) that interact through hydrogen bonds that help to stabilize both GDP and the magnesium ion. Mg1A (olive) is hexacoordinated by water molecules (teal), Ser27 and the O atoms of the terminal β -phosphate group of GDP.

alternates between open and closed conformations depending upon the binding of GDP or GTP, respectively.

3.3. Comparison of the LdRab5a crystal structure with GDP-bound and GTP-bound human Rab5a structures

When superimposed on the GDP-bound human Rab5a form A structure (PDB entry 1tu4; Zhu *et al.*, 2004), the crystal structure of LdRab5a overlaps well in most of the regions apart from the Switch I region (Thr34–Phe50; r.m.s.d. of 0.62 Å over 118 C $^{\alpha}$ atoms). In the GDP-bound HsRab5a structure, helix $\alpha 1$ displays an extra quarter turn, and Switch I and its flanking residues extend from the C-terminus of helix $\alpha 1$ towards the N-terminus of strands $\beta 1$ and $\beta 3$, and then curve towards the N-terminus of the antiparallel strand $\beta 2$. This conformation of Switch I completely exposes the nucleotide-binding site in the HsRab5a structure, as shown in Fig. 4(a) (violet trace). In contrast, in the LdRab5a structure the protein chain turns upwards parallel to helix $\alpha 1$ and then extends towards the C-terminus of strands $\beta 1$ and $\beta 3$, before curving towards the N-terminus of strand $\beta 2$, as highlighted

in Fig. 4(a) (green trace). There is, however, no significant difference in the positioning of the Switch II region between LdRab5a and GDP-bound HsRab5a, as shown in Fig. 4(c).

A superimposition of the LdRab5a structure presented here with the GppNHp-bound HsRab5a structure is shown in Fig. 4(b). The average r.m.s.d. over 122 C $^{\alpha}$ atoms is 0.65 Å. In GppNHp-bound HsRab5a, Switch I and Switch II are together in the closed conformation, which is also referred to as the loaded-spring state. In this conformation, the imidophosphate group is coordinated by Ser29 and Lys33 of the P-loop, Ser51 and Thr52 of Switch I, Gly78 of Switch II and an Mg $^{2+}$ ion. In comparison, Thr45 (equivalent to Thr52 in HsRab5a) of the Switch I region of LdRab5a is displaced 2.6 Å from the closed conformation of HsRab5a. There is also a significant difference in the orientation of Switch II regions between these two structures. Switch II shows significant changes in arrangement of the 70 AGLE 73 region, with a largest displacement of 5 Å for Gly71 and Leu72, followed by Glu73, which is displaced by 4.3 Å. This rearrangement makes Gly71 and Leu72 move away from the nucleotide. In contrast, Glu73 reorients its side chain to move closer to the nucleotide-binding site and

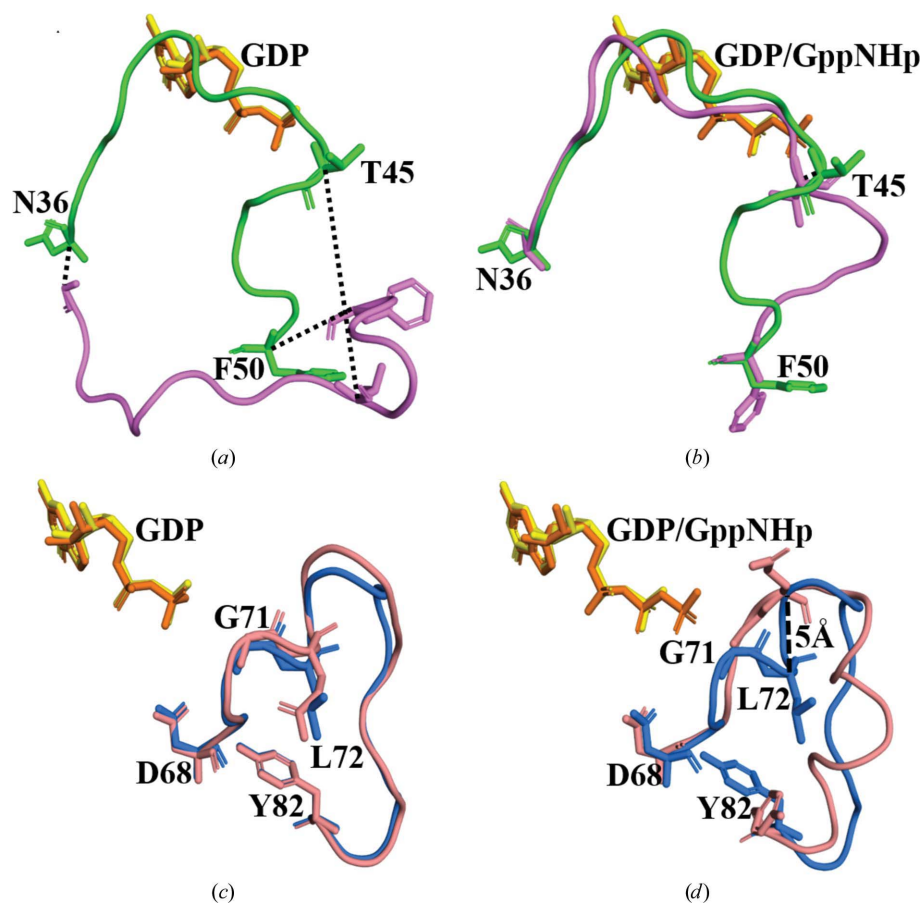


Figure 4

Comparison of the Switch I and II regions of GDP-bound LdRab5a and GDP-bound or GppNHp-bound HsRab5a. (a) Overlap of GDP-bound LdRab5a with GDP-bound form A of HsRab5a, showing the G2 loops containing the Switch I regions as tubes. The side chains of residues that correspond between the two superimposed chains are linked by dashed lines. (b) GDP-bound LdRab5a superimposed with GppNHp-bound HsRab5a, showing the G2 loop regions as tubes. (c) GDP-bound LdRab5a superimposed with GDP-bound HsRab5a, showing the Switch II and helix $\alpha 2$ regions as tubes. (d) GDP-bound LdRab5a superimposed with GppNHp-bound HsRab5a, showing the Switch II region and helix $\alpha 2$ as tubes. Color scheme: green, LdRab5a G2 loop; violet, HsRab5a G2 loop; marine, Switch II and helix $\alpha 2$ of LdRab5a; salmon, Switch II and helix $\alpha 2$ of HsRab5a; yellow, GDP of LdRab5a; orange, GDP/GppNHp of HsRab5a.

interacts with Lys26 of the P-loop and water 128 through its side-chain OE2 (hydrogen-bond distance of 2.7 Å).

3.4. Comparison of the LdRab5a crystal structure with the GDP-bound PfRab5a and GppNHp-bound yeast Rab5a (Ypt51) structures

We further superimposed LdRab5a on GDP-bound PfRab5a and GppNHp-bound yeast Rab5a (Ypt51). The r.m.s.d.s for these overlaps are 1.2 Å over 137 C α atoms and 0.82 Å over 132 C α atoms, respectively. Superimposition of LdRab5a on PfRab5a shows good overlap for the Switch I region up to the γ -phosphate-interacting residue Thr45. The backbone traces of these two protein chains bifurcate at the Rab5-specific region ⁴⁶IGAA⁴⁹, which follows Thr45, as shown in Fig. 5(a). This region shows the largest difference between the GDP-bound LdRab5a and PfRab5a conformations. However, the backbone traces overlap again at Phe50, which incidentally is part of the invariant hydrophobic triad, in combination with Trp67 and Tyr82. This hydrophobic triad acts as an important recognition interface for effector binding.

Besides this, the Switch II residues overlap well in the region ⁶⁷WDTAGLE⁷³, but the overlap is poorer for the following ⁷⁴RFRSLA⁷⁹ region, which corresponds to the elongated helix α 2. However, in the elongated region, the orientation of the side chains remains similar in the LdRab5a and PfRab5a structures, as shown in Fig. 5(c).

Upon comparison of the LdRab5a structure with the GppNHp-bound Ypt51 structure from yeast, it was observed that the C-terminal end of the G2 loop is shifted towards helix α 2 in Ypt51, as shown in Fig. 5(b). The Switch I threonine (Thr44 in Ypt51) is involved in a hydrogen bond to O1G of GppNHp through its backbone amide NH. In addition, Switch II differs in a similar way at the ⁷⁰AGL⁷² segment as seen in the case of HsRab5a–GppNHp. Also, helix α 2 in this active conformation is well formed and consequently shifted inwards, as shown in Fig. 5(d).

In order to highlight the differences in the Switch I and II regions of LdRab5a, human Rab5a, PfRab5a and yeast Rab5a, a superimposition of all of these structures is shown in Fig. 6. As can clearly be seen, the Switch I regions of LdRab5a and PfRab5a are shifted away from the vicinity of Switch II and

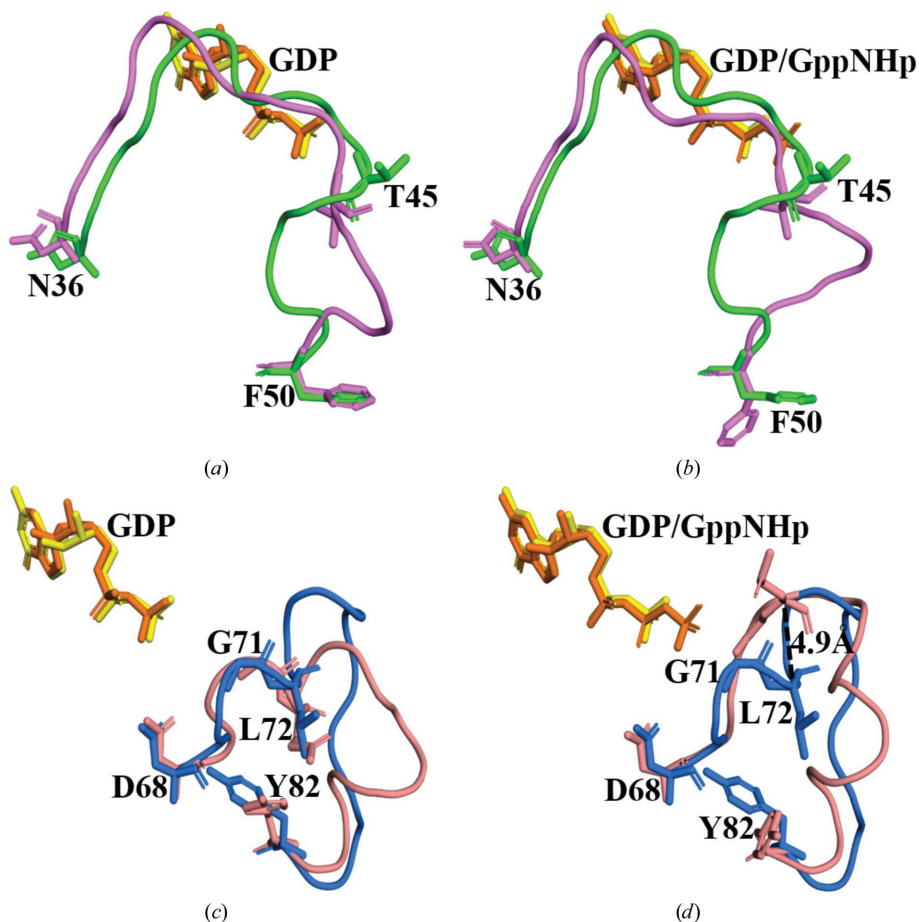


Figure 5

Comparison of the Switch I and II regions of GDP-bound LdRab5a and GDP-bound PfRab5a or GppNHp-bound Ypt51. (a) Overlap of GDP-bound LdRab5a with GDP-bound PfRab5a, showing the G2 loops containing the Switch I regions as tubes. (b) GDP-bound LdRab5a superimposed with GppNHp-bound Ypt51, showing the G2 loop regions as tubes. (c) GDP-bound LdRab5a superimposed with GDP-bound PfRab5a, showing the Switch II and helix α 2 regions as tubes. (d) GDP-bound LdRab5a superimposed with GppNHp-bound Ypt51, showing the Switch II region and helix α 2 as tubes. Color scheme: green, LdRab5a G2 loop; violet, PfRab5a–GDP or yeast Ypt51–GppNHp G2 loop; marine, Switch II and helix α 2 of LdRab5a; salmon, Switch II and helix α 2 of PfRab5a–GDP or yeast Ypt51–GppNHp; yellow, GDP in LdRab5a; orange, GDP/GppNHp in PfRab5a/yeast Ypt51.

towards the N-terminus of strand $\beta 2$, thus forming a crevice between the two switches, in comparison to the HsRab5a and yeast Rab5a structures (Fig. 6*a*). However, the Switch I region of LdRab5a is shifted further towards helix $\alpha 1$ than that in PfRab5a. On the other hand, overlap of the Switch II region, as shown in Fig. 6*b*, displays differences in the nucleotide-binding region of Switch II and the unstructured part of helix $\alpha 2$ in comparison to GppNHp-bound human and yeast Rab5a.

For the various GDP-bound and GTP-bound structures that have been compared above, only weak hydrogen-bond or hydrophobic contacts have been found with the adjacent symmetry-related molecules. In LdRab5a–GDP, Ile46 in the Switch I region forms a hydrogen bond through its backbone carbonyl to the backbone NH2 group of Gly59 of the adjacent

symmetry-mate chain. In GDP-bound PfRab5a, Ile40, Gly41 and Ala42 interact with the side-chain NH2 group of Asn177 of the adjacent symmetry-mate chain through hydrogen bonds, while in GppNHp-bound yeast Rab5a the equivalent Ile40 and Ala42 form hydrogen bonds to the side-chain NH2 group of Lys170 of the symmetry mate. In HsRab5a, Ile53 and Ala55 forms hydrogen bonds to Gly15 of the symmetry mate, while in the LdRab5a Switch II region Ser77 is involved in forming hydrogen bonds to the adjacent symmetry mate in the crystal structure. Further, in LdRab5a, Phe75 is also involved in hydrogen-bond formation to a neighboring symmetry mate. The Switch II residues equivalent to Ser77 and Phe75 of LdRab5a also display similar weak interactions with symmetry-related molecules in the other compared Rab5

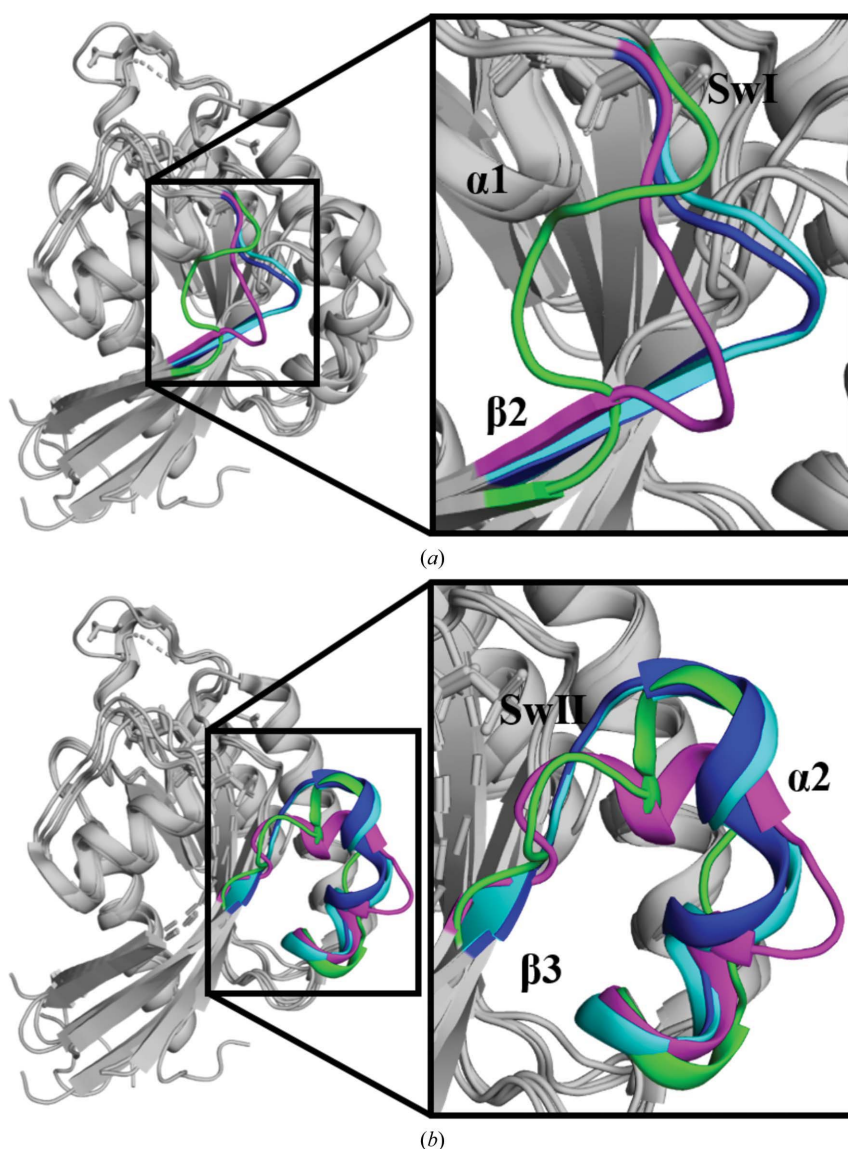


Figure 6 Superimposition of GDP-bound and GppNHp-bound Rab structures. Superimposition and enlarged views of the LdRab5a–GDP (green), PfRab5a–GDP (magenta), Ypt51–GppNHp (blue) and HsRab5a–GppNHp (cyan) structures. (a) Superimposition with expansion of the G2 loop showing the Switch I (SwI) and family-specific ($^{44}\text{TTIGAAF}^{50}$) regions of the GDP-bound LdRab5a and PfRab5a structures and the GppNHp-bound Ypt51 and HsRab5a structures. (b) Superimposition with expansion of the Switch II (SwII) and helix $\alpha 2$ regions of GDP-bound LdRab5a and PfRab5a and of GppNHp-bound Ypt51 and HsRab5a.

Table 2

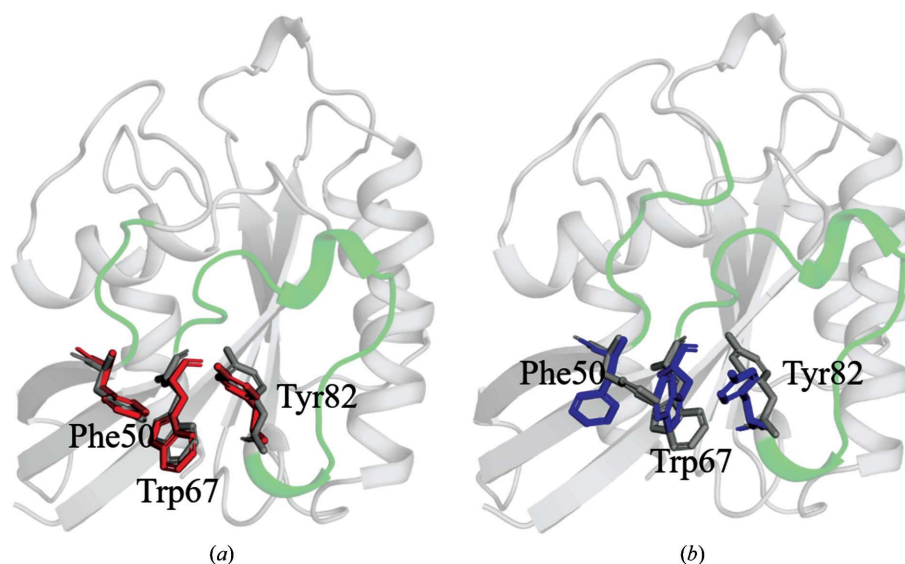
Axis and rotation of invariant aromatic residues between GDP-bound LdRab5a and GppNHp-bound HsRab5a and Ypt51.

Residue	Axis	Angle of rotation (°)	
		Ypt51–GppNHp	HsRab5a–GppNHp
Phe50	CG–CB–CG	109.7	108.1
Trp67	CE3–CG–CE3	66.3	60.1
Tyr82	CG–CB–CG	100.8	104.3

structures. For example, Arg68 in yeast Ypt51, which is at a position equivalent to that of Phe75 in LdRab5a, is involved in hydrogen-bond interactions with its symmetry mate.

3.5. Comparison of the invariant hydrophobic triad

Along with the switch and inter-switch regions, the invariant hydrophobic triad has also been identified as an important effector-binding interface in Rab proteins. This region is comprised of residues Phe50, Tyr82 and Trp67 (numbering as per the stabilized LdRab5a sequence). As described above, Phe50 follows the Rab5-specific ⁴⁶IGAA⁴⁹ region, and the protein chain of Rab5a once again superimposes with those of PfRab5a and yeast Rab5a at this residue after bifurcating at Thr45 in Switch I. However, the invariant phenylalanine is seen to rotate by around 109.7° along the CG–CB–CG bond axis. A similar rotation is observed for Trp67 and Tyr82 between the GDP-bound and GTP-bound Rab5a structures discussed above. The overlap of GDP-bound LdRab5a and PfRab5a, highlighting the invariant hydrophobic triad, is shown in Fig. 7(a), while a superimposition of GDP-bound LdRab5a and GppNHp-bound yeast Rab5a is shown in Fig. 7(b). The degree of rotation with reference to the GDP-bound LdRab5a for these three residues is given in Table 2.


Figure 7

Rotameric orientation comparison of conserved hydrophobic triad residues. (a) Superimposed cartoon and stick model views showing the orientation of the conserved hydrophobic triad residues (Phe50, Trp67 and Tyr82) in the LdRab5a (gray) and PfRab5a (red) structures. (b) Superimposed cartoon and stick model views showing the orientation of the conserved hydrophobic triad residues (Phe50, Trp67 and Tyr82) in the LdRab5a (gray) and Ypt51–GppNHp (blue) structures.

From the above results, it can be seen that nucleotide exchange from GDP to GTP induces allosteric conformational changes through the switch and inter-switch regions, which are the primary site of effector recognition and binding. Surface representations of various Rab proteins with highlighted Switch I, inter-switch, Switch II and helix $\alpha 2$ regions are shown in Fig. 8. As can be seen from the surface representation, these regions remain separated from each other in the GDP-bound conformation (Fig. 8a). On the other hand, these regions come closer to one another on the binding of a nucleotide triphosphate. In the GppNHp-bound form they combine to form an interacting interface or epitope, which displays a high degree of structural similarity, as shown in Fig. 8(b).

3.6. Molecular-dynamics simulations

An interesting aspect of Rab proteins in the GDP-bound state is their interaction with GEF proteins. GEF proteins stimulate the release of GDP, and structures of GEF bound to nucleotide-free Rab proteins have been determined (Uejima *et al.*, 2010; Delprato & Lambright, 2007). GTP competes with GEF for the nucleotide-free Rab. We performed MD simulations of LdRab5a–GDP and nucleotide-free apo LdRab5a, using the crystal structure presented here as a starting point, in order to map the possible conformational changes on going from the GDP-bound to the nucleotide-free state, which is an intermediate between the inactive GDP-bound form and the activated GTP-bound form. Plots of trajectories during 100 ns simulations show that the r.m.s.d. values of the protein in the GDP-bound conformation are lower than those of the nucleotide-free form of the protein throughout the simulation, as shown in Fig. 9(a). This depicts the higher stability of the GDP-bound form of LdRab5a in comparison to the protein alone. An analysis of r.m.s.f. values plotted against residue

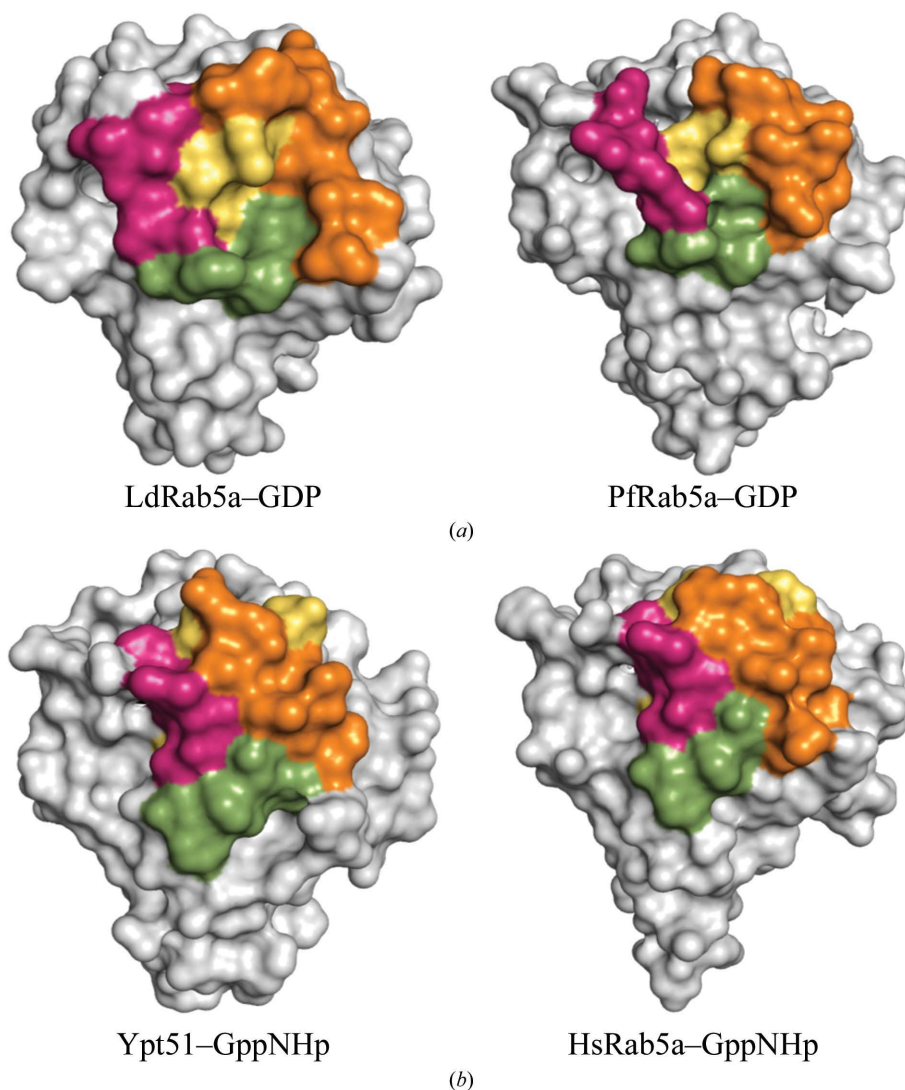


Figure 8 Surface view of the GDP-bound and GppNHp-bound conformations showing changes in the effector-binding interface. (a) Conformational organization of the Switch I (pink), inter-switch (green), Switch II (gold) and helix $\alpha 2$ (orange) regions in GDP-bound LdRab5a and PfRab5a. (b) Conformational organization of the Switch I (pink), inter-switch (green), Switch II (gold) and helix $\alpha 2$ (orange) regions in GppNHp-bound Ypt51 and HsRab5a.

number shows that the residues in the switch regions, and also in other loop regions, exhibit higher fluctuations in nucleotide-free LdRab5a. This might allow GTP to access the active site. Moreover, the GDP-interacting residues were stable and showed an r.m.s.f. around the baseline in the simulation run of GDP-bound LdRab5a, as shown in Fig. 9(b). Additionally, upon comparing the simulated structure in the presence of GDP with the input crystal structure after every 10 ns interval, we found gradual change in flexibility over the 100 ns simulation.

4. Discussion

In the endocytic pathway, Rab5 is present in sorting endosomes, whereas Rab4 and Rab11 are localized in recycling endosomes. Rab7, Rab9 and Rab24 are associated with the late endosomal compartment (Wandinger-Ness & Zerial, 2014). Rab5 controls endosome biogenesis, maturation and fusion through multiple effectors. The *Leishmania* parasite

possess two Rab5 isoforms, which have been reported to function in early endosome formation and targeting. LdRab5a and LdRab5b are essential proteins. LdRab5a induces FPE, but also enhances the kinetics of lysosomal transport (Rastogi *et al.*, 2016). *Leishmania* endocytoses hemoglobin (Hb) through a specific Hb receptor located in the flagellar pocket. Rapid receptor-mediated endocytosis is regulated by LdRab5b. Endocytosed Hb is degraded in the lysosomes via Rab7-dependent processes to generate intracellular heme, which is essential for the parasite (Patel *et al.*, 2008). It is imperative that the two LdRab5 proteins execute their roles by binding to their specific effectors. Mass-spectrometric analysis of the interactome of LdRab5a and LdRab5b indicated 32 and 26 exclusive binding partners, respectively, for these proteins (Rastogi *et al.*, 2016). Dynein, kinesin and tubulin were identified as some common LdRab5 interactors, and these proteins have also been shown to regulate endocytosis and vesicular trafficking. Although the interactome analysis did not reveal homologs of any of the

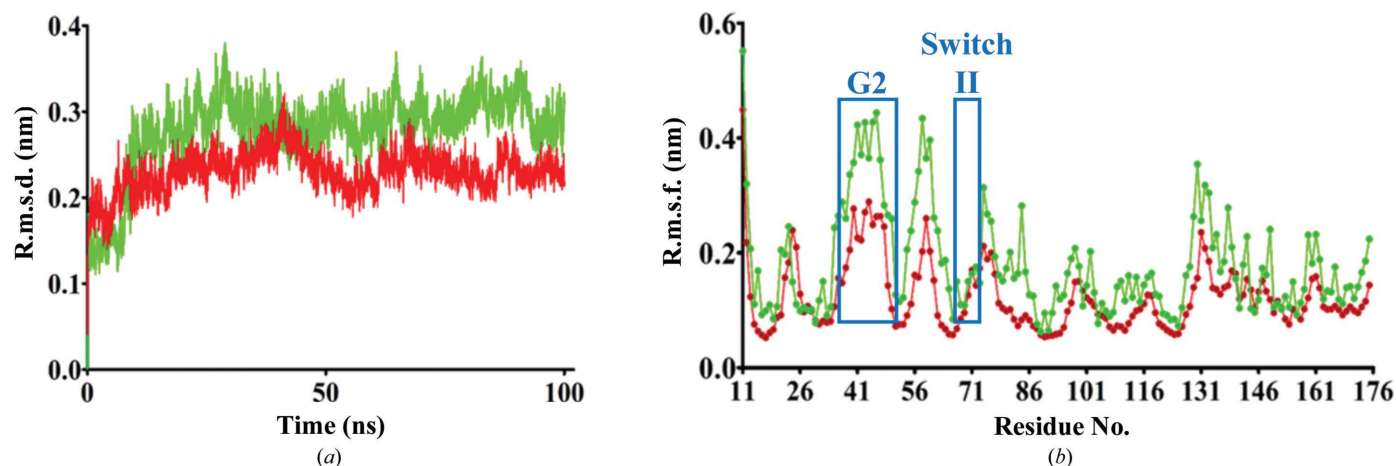


Figure 9
MD simulations of LdRab5a in the presence (red) and absence (green) of GDP. (a) R.m.s.d. comparison for apo and GDP-bound LdRab5a over 100 ns of MD simulations. (b) Per-residue backbone r.m.s.f. comparison for apo and GDP-bound LdRab5a over 100 ns of MD simulations. R.m.s.f. values for residues representing the G2 loop (which includes the Switch I region) and Switch II regions are enclosed in blue boxes.

conventional mammalian Rab5 effectors such as EEA1, rabaptin-5 or rabenosyn-5, it is nevertheless interesting to look at the binding modes of these effectors to Rab5. Structures of all of these effectors have been determined in complex with human Rab5 (Rastogi *et al.*, 2016). Early endosomal autoantigen 1 (EEA1) enhances endosome fusion. EEA1 is a long coiled-coil homodimer with an N-terminal C2H2 zinc finger (ZF) and a C-terminal FYVE domain. A contiguous surface of the EEA1 C2H2 ZF formed by residues from the $\beta 1$ – $\beta 2$ strands, $\alpha 1$ helix and a short N-terminal extension binds to the switch and inter-switch regions of Rab5 through a predominantly nonpolar interface augmented by polar interactions (Mishra *et al.*, 2010). Rabaptin-5 is an essential and rate-limiting component of early endosome fusion. It is recruited to early endosome and endocytic vesicle membranes by Rab5 in a GTP-dependent manner and is involved in both heterotypic and homotypic early endosome fusion. Rabaptin-5 binds specifically to Rab5 with its C-terminal region, which consists of a helix of ~ 36 residues followed by a tight loop and a short helix. Rab5 mainly uses its Switch II and inter-switch (that is $\beta 2$ and $\beta 3$) regions to contact rabaptin-5 (Zhu *et al.*, 2004). Rabenosyn-5 binds to Rab22, which is a member of the Rab5 phylogenetic group, through a helical hairpin. The interaction site on Rab22 is again the switch and inter-switch regions (Eathiraj *et al.*, 2005). In fact, the binding sites of human Rab5 for various effectors exhibit a large degree of overlap, irrespective of the topology of the effector. At the same time, the Rab5 interaction sites on these effectors also exhibit a high degree of physiochemical similarity, indicating convergent evolution. The main feature of the Rab5–effector interface is the shape complementarity of primarily nonpolar surfaces, especially to engage Phe50 in Switch I, Phe75 in Switch II, Leu78 and Ile81. The interface also has features to complementarily accommodate the polar groups of the binding partners. Perhaps as a result of this convergent evolution, Rab5 exhibits high affinity towards its cognate effector partner. For example, the EEA1 C2H2 zinc-finger domain exhibits the highest affinity for Rab5, a seven-

fold lower affinity for the phylogenetically similar Rab22 and an almost 100-fold lower affinity for 30 other Rabs (Mishra *et al.*, 2010).

The *Leishmania* Rabs display 30–50% sequence similarity to higher eukaryotic Rab proteins. They retain the GTPase fold and the conserved loops and residues. While the structure of GTP-bound LdRab5a remains to be determined, it is worthwhile discussing the anticipated conformational changes in the switch and inter-switch regions upon nucleotide exchange. The GDP-binding conformation of LdRab5a is clear from the current study, while the GTPase activity of LdRab5a has previously been characterized (Rastogi *et al.*, 2016). Structural comparisons indicate that several conserved and some less conserved regions change in orientation upon nucleotide exchange and play pivotal roles in interactions with specific binding partners (Pylypenko *et al.*, 2018). One major change is the movement of the conserved Thr45 in the Switch I region away from the nucleotide moiety in the GDP-bound inactive conformation. It can be anticipated that upon GTP binding this residue will move closer to the γ -phosphate group and its backbone amide NH will interact with an O atom of the γ -phosphate. It can also be anticipated that the segment following Thr45, $^{46}\text{IGAA}^{49}$, will adopt a conformation similar to that seen for GppNHp-bound HsRab5a and yeast Ypt51 (Zhu *et al.*, 2003; Esters *et al.*, 2000). Concomitantly, the Switch II residues $^{71}\text{GLE}^{73}$ would shift by ~ 5 Å and rearrange upon GTP binding, enabling interaction between the NH group of Gly71 and an O atom of the γ -phosphate group. This movement of the $^{71}\text{GLE}^{73}$ segment is facilitated by the reformation of helix $\alpha 2$, which is split and elongated in the GDP-bound state. Upon reformation, helix $\alpha 2$ will move closer to the C-terminus of the G2 loop. Overall, upon GTP binding, the Switch I and Switch II regions would together adopt the closed loaded-spring conformation, along with a reorientation of the invariant hydrophobic triad residues. In LdRab5a, Gln72 has been replaced by leucine to decrease the intrinsic GTPase activity. The conserved Gln72 catalyzes the hydrolysis of GTP by assisting the nucleophilic attack by a water molecule on the

bond between the terminal β -phosphoryl and γ -phosphoryl groups (Pai *et al.*, 1990). Further, upon GTP hydrolysis, Gln72 is oriented in such a way so as to enable interaction between the conserved Lys26 of the P-loop and an aspartate residue of GEF, which leads to the exchange of GDP for GTP (Lange-meyer *et al.*, 2014; Delprato & Lambright, 2007; Delprato *et al.*, 2004).

We are currently trying to crystallize LdRab5a bound to GppNHP in order to map the allosteric changes associated with nucleotide exchange. As mentioned above and in previous reports, effectors of *Leishmania* Rab5 isomers have not been identified to date. We have searched the genome sequence of *L. donovani* for effector proteins with Rab5-specific binding domains. However, determinants of specificity can only be established through experimental characterization.

5. Conclusion

We have determined the crystal structure of the stabilized GTPase domain of the *L. donovani* Rab5a protein in the GDP-bound state at 1.80 Å resolution. LdRab5a displays a canonical Rab fold, with the P-loop, Switch I and Switch II being regions of high functional relevance. In the structure, the conserved Thr45 residue of the G2 loop or Switch I region moves away from the nucleotide and the following residues trace a unique path up to Phe50. The residues ⁷⁰AGLQ⁷³ of the Switch II region are shifted by up to 5 Å from the anticipated loaded-spring conformation, with helix $\alpha 2$ being split and elongated in the ⁷⁴RFRSL⁷⁹ segment. The invariant hydrophobic triad residues were found to have rotated away from their anticipated conformation in the GTP-bound state. The structural characterization of LdRab5a will be helpful in unraveling the allosteric changes upon nucleotide exchange and may help in understanding the specificity of LdRab5a towards its effectors.

Acknowledgements

We are grateful to the X-ray Diffraction Facility, National Institute of Immunology, New Delhi, India. MZ is grateful to the Academy of Scientific and Innovative Research (AcSIR) for PhD registration. This is communication number 10131 from CSIR-CDRI, Lucknow.

Funding information

The research leading to these results, in part, received funding from UK Research and Innovation via the Global Challenges Research Fund under grant agreement 'A Global Network for Neglected Tropical Diseases' (grant No. MR/P027989/1). MZ is the recipient of a research fellowship from the Council of Scientific and Industrial Research (CSIR), New Delhi, India.

References

Anant, J. S., Desnoyers, L., Machius, M., Demeler, B., Hansen, J. C., Westover, K. D., Deisenhofer, J. & Seabra, M. C. (1998). *Biochemistry*, **37**, 12559–12568.

Blümer, J., Rey, J., Dehmelt, L., Mazel, T., Wu, Y.-W., Bastiaens, P., Goody, R. S. & Itzen, A. (2013). *J. Cell Biol.* **200**, 287–300.

Brünger, A. T. (1993). *Acta Cryst.* **D49**, 24–36.

Chauhan, I. S., Kaur, J., Krishna, S., Ghosh, A., Singh, P., Siddiqi, M. I. & Singh, N. (2015). *BMC Evol. Biol.* **15**, 261.

Delprato, A. & Lambright, D. G. (2007). *Nat. Struct. Mol. Biol.* **14**, 406–412.

Delprato, A., Merithew, E. & Lambright, D. G. (2004). *Cell*, **118**, 607–617.

Doherty, G. J. & McMahon, H. T. (2009). *Annu. Rev. Biochem.* **78**, 857–902.

Eathiraj, S., Pan, X., Ritacco, C. & Lambright, D. G. (2005). *Nature*, **436**, 415–419.

Emsley, P. & Cowtan, K. (2004). *Acta Cryst.* **D60**, 2126–2132.

Emsley, P., Lohkamp, B., Scott, W. G. & Cowtan, K. (2010). *Acta Cryst.* **D66**, 486–501.

Esters, H., Alexandrov, K., Constantinescu, A. T., Goody, R. S. & Scheidig, A. J. (2000). *J. Mol. Biol.* **298**, 111–121.

Gavriljuk, K., Itzen, A., Goody, R. S., Gerwert, K. & Kötting, C. (2013). *Proc. Natl Acad. Sci. USA*, **110**, 13380–13385.

Goody, R. S., Müller, M. P. & Wu, Y.-W. (2017). *Biol. Chem.* **398**, 565–575.

Guo, Z., Hou, X., Goody, R. S. & Itzen, A. (2013). *J. Biol. Chem.* **288**, 32466–32474.

Hutagalung, A. H. & Novick, P. J. (2011). *Physiol. Rev.* **91**, 119–149.

Jancarik, J. & Kim, S.-H. (1991). *J. Appl. Cryst.* **24**, 409–411.

Kořený, L., Lukeš, J. & Oborník, M. (2010). *Int. J. Parasitol.* **40**, 149–156.

Langemeyer, L., Nunes Bastos, R., Cai, Y., Itzen, A., Reinisch, K. M. & Barr, F. A. (2014). *eLife*, **3**, e01623.

Langemeyer, L., Perz, A., Kümmel, D. & Ungermann, C. (2018). *J. Biol. Chem.* **293**, 731–739.

Laskowski, R. A., MacArthur, M. W., Moss, D. S. & Thornton, J. M. (1993). *J. Appl. Cryst.* **26**, 283–291.

Leung, K. F., Baron, R. & Seabra, M. C. (2006). *J. Lipid Res.* **47**, 467–475.

Liebschner, D., Afonine, P. V., Baker, M. L., Bunkóczi, G., Chen, V. B., Croll, T. I., Hintze, B., Hung, L.-W., Jain, S., McCoy, A. J., Moriarty, N. W., Oeffner, R. D., Poon, B. K., Prisant, M. G., Read, R. J., Richardson, J. S., Richardson, D. C., Sammito, M. D., Sobolev, O. V., Stockwell, D. H., Terwilliger, T. C., Urzhumtsev, A. G., Videau, L. L., Williams, C. J. & Adams, P. D. (2019). *Acta Cryst.* **D75**, 861–877.

Maheshwari, D., Yadav, R., Rastogi, R., Jain, A., Tripathi, S., Mukhopadhyay, A. & Arora, A. (2018). *Biophys. J.* **115**, 1217–1230.

Markgraf, D. F., Peplowska, K. & Ungermann, C. (2007). *FEBS Lett.* **581**, 2125–2130.

Matthews, B. W. (1968). *J. Mol. Biol.* **33**, 491–497.

McCoy, A. J., Grosse-Kunstleve, R. W., Adams, P. D., Winn, M. D., Storoni, L. C. & Read, R. J. (2007). *J. Appl. Cryst.* **40**, 658–674.

Mishra, A., Eathiraj, S., Corvera, S. & Lambright, D. G. (2010). *Proc. Natl Acad. Sci. USA*, **107**, 10866–10871.

Murshudov, G. N., Skubák, P., Lebedev, A. A., Pannu, N. S., Steiner, R. A., Nicholls, R. A., Winn, M. D., Long, F. & Vagin, A. A. (2011). *Acta Cryst.* **D67**, 355–367.

Orrego, L. M., Cabello-Donayre, M., Vargas, P., Martínez-García, M., Sánchez, C., Pineda-Molina, E., Jiménez, M., Molina, R. & Pérez-Victoria, J. M. (2019). *FASEB J.* **33**, 13367–13385.

Pai, E. F., Kregel, U., Petsko, G. A., Goody, R. S., Kabsch, W. & Wittinghofer, A. (1990). *EMBO J.* **9**, 2351–2359.

Patel, N., Singh, S. B., Basu, S. K. & Mukhopadhyay, A. (2008). *Proc. Natl Acad. Sci. USA*, **105**, 3980–3985.

Pylypenko, O., Hammich, H., Yu, I.-M. & Houdusse, A. (2018). *Small GTPases*, **9**, 22–48.

Qin, X., Wang, J., Wang, X., Liu, F., Jiang, B. & Zhang, Y. (2017). *Drug Discov. Today*, **22**, 1139–1147.

- Rastogi, R., Verma, J. K., Kapoor, A., Langsley, G. & Mukhopadhyay, A. (2016). *J. Biol. Chem.* **291**, 14732–14746.
- Real, F. & Mortara, R. A. (2012). *PLoS Negl. Trop. Dis.* **6**, e1518.
- Schmid, N., Eichenberger, A. P., Choutko, A., Riniker, S., Winger, M., Mark, A. E. & van Gunsteren, W. F. (2011). *Eur. Biophys. J.* **40**, 843–856.
- Sengupta, S., Tripathi, J., Tandon, R., Raje, M., Roy, R. P., Basu, S. K. & Mukhopadhyay, A. (1999). *J. Biol. Chem.* **274**, 2758–2765.
- Stenmark, H. & Olkkonen, V. M. (2001). *Genome Biol.* **2**, reviews3007.1.
- Uejima, T., Ihara, K., Goh, T., Ito, E., Sunada, M., Ueda, T., Nakano, A. & Wakatsuki, S. (2010). *J. Biol. Chem.* **285**, 36689–36697.
- Ullrich, O., Horiuchi, H., Bucci, C. & Zerial, M. (1994). *Nature*, **368**, 157–160.
- Vetter, I. R. & Wittinghofer, A. (2001). *Science*, **294**, 1299–1304.
- Wandinger-Ness, A. & Zerial, M. (2014). *Cold Spring Harb. Perspect. Biol.* **6**, a022616.
- Young, J. & Kima, P. E. (2019). *Yale J. Biol. Med.* **92**, 511–521.
- Zahraoui, A., Touchot, N., Chardin, P. & Tavitian, A. (1989). *J. Biol. Chem.* **264**, 12394–12401.
- Zhu, G., Liu, J., Terzyan, S., Zhai, P., Li, G. & Zhang, X. C. (2003). *J. Biol. Chem.* **278**, 2452–2460.
- Zhu, G., Zhai, P., Liu, J., Terzyan, S., Li, G. & Zhang, X. C. (2004). *Nat. Struct. Mol. Biol.* **11**, 975–983.